J. Fluid Mech. (1993), *vol.* 248, *pp.* 567–581

The plane symmetric sudden-expansion flow at low Reynolds numbers

By F. DURST, J. C. F. PEREIRA† AND C. TROPEA

Lehrstuhl für Strömungsmechanik, Universität Erlangen-Nürnberg, Cauerstr. 4, D-8520 Erlangen, Germany

(Received 20 April 1989 and in revised form 5 August 1992)

Detailed velocity measurements and numerical predictions are presented for the flow through a plane nominally two-dimensional duct with a symmetric sudden expansion of area ratio 1:2. Both the experiments and the predictions confirm a symmetry-breaking bifurcation of the flow leading to one long and one short separation zone for channel Reynolds numbers above 125, based on the upstream channel height and the maximum flow velocity upstream. With increasing Reynolds numbers above this value, the short separated region remains approximately constant in length whereas the long region increases in length.

The experimental data were obtained using a one-component laser-Doppler anemometer at many Reynolds number values, with more extensive measurements being performed for the three Reynolds numbers 70, 300 and 610. Predictions were made using a finite volume method and an explicit quadratic Leith type of temporal discretization. In general, good agreement was found between measured and predicted velocity profiles for all Reynolds numbers investigated.

1. Introduction

It is well known that the flow through a plane symmetric sudden expansion becomes asymmetric about the central plane as the Reynolds number is increased. This was experimentally documented by Durst, Melling & Whitelaw (1974), Chedron, Durst & Whitelaw (1978), Sobey (1985) and more recently by Fearn, Mullin & Cliffe (1990). At low Reynolds numbers the flow remains symmetric with separation regions of equal length on either side of the channel, this length increasing with increasing Reynolds number. At higher Reynolds numbers, however, one recirculation region increases in length at the expense of the other recirculation zone and the asymmetry remains in the flow, even up to turbulent flow conditions (Restivo & Whitelaw 1978). This phenomenon is explained by a 'Coanda' effect, see Wille & Fernholz (1965) and Shapira, Degani & Weihs (1990).

The critical Reynolds number Re_c at which the asymmetry begins is not well-defined experimentally and results from Fearn *et al.* (1990) and the present study suggest that this is not a sudden transition, and possibly due to small imperfections present in the experimental apparatus. In any case, past experimental investigations suggest that the Reynolds number at which asymmetry is observed is also influenced by the channel expansion ratio, k_e, and aspect ratio k_a. Although systematic dependencies have not yet been established, the Re_c value decreases with increasing expansion ratio and decreases with an increase in channel aspect ratio.

† Present address: Instituto Superior Técnico, Department of Mechanical Engineering, Av. Rovisco Pais, Lisbon, Portugal.

The plane sudden expansion was numerically investigated by Acrivos & Schrader (1982), in which the dependence of the separation length on the Reynolds number and on the ratio of the upstream channel half-width to the step height was investigated in the limit of large Reynolds numbers. It was found that the separation length was proportional to Reynolds number when the inlet profile was fully developed. When a uniform inlet velocity profile was considered, there was a critical ratio at which this linear growth disappeared. Other fundamental studies were performed by Sobey (1985) and Sobey & Drazin (1986), who investigated the instabilities and bifurcations of two-dimensional channel flows. At a relatively low critical Reynolds number, a pitchfork bifurcation occurred such that two stable asymmetric steady flows were formed. Increasing the Reynolds number allowed several steady and unsteady solutions and when the Reynolds number was sufficiently large a Hopf bifurcation existed, resulting in solutions periodic in time. However, the smooth channel expansion and the periodicity in the longitudinal direction prevents these conclusions from being applied to the present flow geometry.

Recently Shapira *et al.* (1990) have performed a linear stability analysis of the symmetric flow in sudden plane expansions showing that the eigenvalue which corresponds to the least stable mode is real, indicating that for Reynolds numbers larger than a critical value steady asymmetric solutions exist. They computed a critical Reynolds number (Re_c) that is in good agreement with the one observed experimentally for an expansion ratio of 1:3 but they overpredicted Re_c for the expansion ratio 1:2.

The objective of this work is twofold. First to map in detail using laser–Doppler velocimetry (LDV) the flow field in a channel with an expansion ratio 1:2 at a high Reynolds number, in the fully laminar regime (up to $Re = 610$, based on upstream channel height and upstream maximum velocity) and in the absence of strong induced flow three-dimensionality or unsteadiness. Second, to obtain numerical predictions using third-order temporal and spatial finite difference discretization schemes. Special emphasis is given to the calculation of the onset of flow asymmetry and to the possibility of transition of the flow to a time-dependent behaviour at high laminar Reynolds numbers via a two-dimensional (Hopf) bifurcation.

In §2 of the present paper, the experimental set-up and the measuring system employed in the present study are described, together with some measurements that characterize the overall features of the flow. At high Reynolds numbers the flow showed a slight three-dimensionality throughout the separation region, which is also documented. In §3 details of the computational method are given. The details of the temporal and spatial discretization are given in the Appendix. Results of the experimental and numerical work are presented and discussed in §4, with particular attention being given to the strong asymmetry that characterizes this flow. Direct comparisons between measurements and predictions are made in this section, showing good overall agreement.

2. Experimental details

The experiments were conducted in the facility sketched in figure 1. In the centre of the figure the test section is shown, indicating the plane symmetric two-dimensional duct with a sudden change in cross-sectional area yielding an expansion ratio of 1 to 2. The aspect ratio of the channel was 16:1 and 8:1 before and after the expansion, respectively. The sidewalls, constructed of glass, allowed optical access from both sides of the channel for all values of x upstream and downstream of the

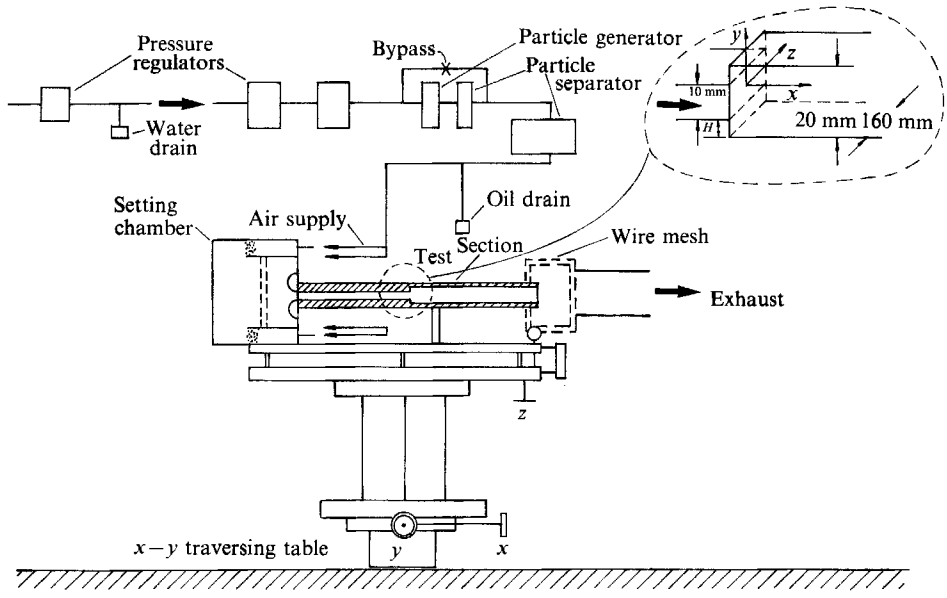

FIGURE 1. Experimental equipment and test section.

expansion, thus allowing the application of the laser–Doppler measuring technique. Spacers of equal height were positioned around the tightening screws and between the upper and lower sidewalls to maintain a constant channel height before and after the expansion ($\pm 1\%$). To carry out traverses of the measurement volume, the test section was placed on a three-dimensional traversing table fitted with precision dial gauges allowing the position of the measuring control volume to be located within ± 15 μm in the x- and z-directions and ± 5 μm in the y-direction.

To provide a constant air flow, compressed air from the air supply line of the laboratory was passed through a first and second stage pressure regulator which controlled the outgoing pressure to within $\pm 0.15\%$. This provided an air stream of sufficiently constant supply pressure to ensure good repeatability of the flow settings. It also provided a constant supply to the atomizers which produced seeding droplets. A droplet separator was placed after the atomizer to remove the large droplets and to yield a particle size distribution suitable for the present measurements. The air stream with particles was passed through a second separator and into the settling chamber of the test section where it flowed through screens and flow straighteners prior to reaching the contraction nozzle of the test section inlet. Owing to the large dimensions of the settling chamber very low streamwise velocities occurred, resulting in a residence time sufficiently long to create a particle-free zone in the upper part of the test section. To obtain measurements of both the short and the long separation regions, the flow was investigated both for situations where the shorter separation bubble had settled on the lower wall and where the larger separation bubble settled on the lower wall. It was observed during preliminary experiments that either the smaller or the larger separation region could settle on either side of the flow, see Chedron *et al.* (1978). Irrespective of which side the attachment occurred, the corresponding short and long separation regions always had identical dimensions.

In order to prevent laboratory air draughts from influencing the flow through the channel, the outlet was closed with a wire mesh box. The downstream end of the box was connected to a suction pipe that vented the air out of the laboratory. Filter

material and flow straighteners were placed in the exhaust pipe to suppress any disturbing influences of the exhaust fan. Measurements of the flow velocity at the outlet of the channel were recorded as a time series and as frequency spectra for very low-velocity channel flows, approximately 1 cm/s, in order to demonstrate that there was no periodic fluctuations of velocity due to the suction fan on the exhaust side.

The laser–Doppler anemometer (LDA) for the velocity measurements consisted of a 15 mW helium–neon laser, a self-aligning beam splitter and a double Bragg cell unit all mounted on a common base to form a single-channel laser–Doppler optics operating in the forward scatter mode. The scattered light was collected through a single lens element and focused onto a pinhole in front of the photomultiplier, laid out to provide an effective measuring control volume of 150 μm in diameter and about 1 mm in length. The signal from the photomultiplier was processed by a BBC-Goerz frequency tracker which was operated with a signal rate of approximately 60% by appropriately adjusting the particle-seeding bypass system. The analog output signal of the tracker was digitized using a 12-bit A/D and read into a Hewlett-Packard 2100 computer, which allowed mean velocity and fluctuating velocities to be computed.

The data presented in this paper relate to the mean velocity measurements. The r.m.s. velocity measurements were low and could all be explained by gradient broadening effects due to the finite size of the measuring control volume. Some higher-amplitude velocity fluctuations, amounting to 1% of the mean inlet flow velocity, could be detected near the main reattachment points for the Reynolds number 610. At $Re = 300$ these fluctuations did not exceed 0.5% of the inlet mean velocity. Therefore, oscillations of the type observed by Sobey (1985) or Sobey and Drazin (1986) and Fearn *et al.* (1990) were not observed in this experiment. The mass flow, as computed by integrating the mean velocity profiles taken on the channel centreline, lay within $\pm 2\%$ of the value computed at the inlet for all measurement planes considered.

A fully developed laminar flow (parabolic profile) was achieved prior to and far downstream of the expansion. The possible three-dimensionality was investigated in two ways. Oil film studies were performed to visualize the extent of the corner vortex found in the sidewall region of the test section. This vortex extended between 1 and 1.5 step heights into the flow for $Re = 70$ and was therefore considered to have only a small influence on the centre part of the flow. Further study of the three-dimensionality consisted of velocity profiles obtained across the width of the channel at selected downstream positions. Figure 2 illustrates the contours dividing positive U-velocities from negative U-velocities in a channel cross-section at $Re = 610$. In this case the corner vortices, indicated approximately by the hatched regions, have increased in size from those measured for lower Reynolds number.

Detachment and reattachment points of the flow were determined by measuring the $U = 0$ position at various distances from the wall and extrapolating this line to the wall surface. These positions, denoted by $x_1, x_2 \ldots$, are normalized with the step height of the expansion, S.

3. Numerical method

The flow through the sudden expansion is assumed to be laminar, two-dimensional, steady or time dependent and the fluid to be Newtonian, incompressible and of constant viscosity. A finite volume method was used to discretize the Navier–Stokes

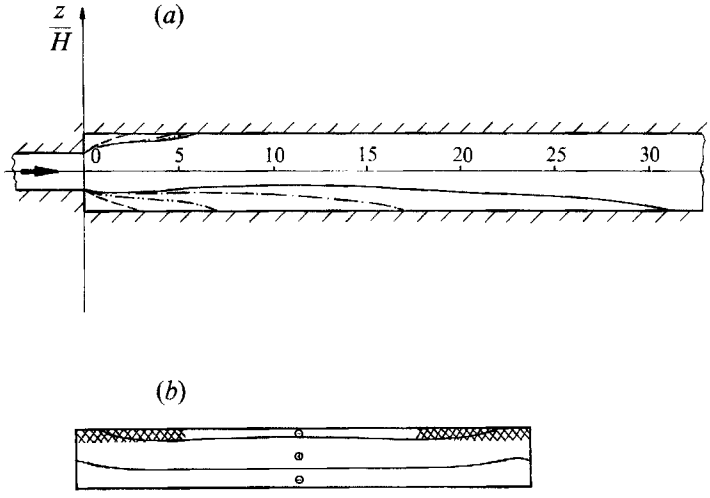

FIGURE 2. Lines of $U = 0$ in (a) the (x, y)-plane and (b) the (y, z)-plane at $X/H = 3.6$ for $Re = 610$ (——), $Re = 300$ (—·—), $Re = 150$ (—· ·—) and $Re = 70$ (– –).

equations. A temporal flow evolution was originated by impulsively starting the flow from rest. Predictions obtained with three different temporal discretization schemes were compared to investigate if the temporal accuracy would greatly influence the predictions. The schemes used were the first-order implicit backward Euler scheme; the second-order-accurate Crank–Nicolson and the third-order explicit quadratic Leith type (QUICKEST) (Leonard 1979). Common to all the numerical algorithms was the use of a 13-point quadratic upstream scheme for convection–diffusion discretization. The derivation of the QUICKEST scheme was presented by Leonard (1979) for one-dimensional problems. Its extension to multidimensional problems is not straightforward and very few predictions have been reported using this scheme, see Davis & Moore (1982). Details using a new derivation procedure are provided in the Appendix where the finite difference counterparts of the Navier–Stokes equations in two-dimensional form are presented. Although some differences were found in the three numerical solutions, they influence neither the physical analysis of the flow nor the comparison with experiments for the steady-state solution.

The flow was impulsively started from rest with inlet conditions corresponding to a fully developed channel flow prescribed at $x/H = -4$. At the outlet ($x/H = 100$) a monochromatic travelling wave was assumed to describe the open boundary, i.e.

$$\frac{\partial \phi}{\partial t} + c\frac{\partial \phi}{\partial x} = 0, \tag{1}$$

where $\phi = U, V$, and c denotes the wave celerity taken as the channel bulk velocity. If a steady state is reached, this boundary condition reverts to zero velocity gradient. No-slip conditions were set at the channel boundaries. As a staggered grid was used, the convective and diffusive fluxes across the control volume half-face surrounding the sharp edge corners at the plane expansion were evaluated according to Davis & Moore (1982).

Computations were performed on two grids comprising 56×56 and 112×112 control volumes respectively. Solution error estimates were obtained as suggested by Obi, Peric & Scheuerer (1990) yielding a maximum absolute error of 5% of the 112×112 grid. All subsequent results presented were obtained using this grid.

For explicit calculations the maximum Courant number was kept below 0.8 yielding a time step equal to $\Delta t = 10^{-4}$ s for $Re = 610$, or a non-dimensionalized time step ($\Delta t\, U_{\max}/H = 9 \times 10^{-3}$).

In neither the experiment nor the predictions is the exact origin of the flow bifurcation trigger clear. Fearn *et al.* (1990), for instance, postulated that small imperfections which are inevitably present in the experimental apparatus, prohibit a symmetric bifurcation velocity diagram. They modelled these imperfections by computing a slightly asymmetric expansion (1 %). In the present work a symmetric flow configuration was always assumed and a flow bifurcation occurred without any geometric inlet perturbation. This is due to truncation errors which prevent a zero transverse velocity at the symmetry plane. Traverse velocity leads to a locally higher streamwise velocity and thus a low pressure that maintains the asymmetric flow through the cross-channel pressure gradient.

In the vicinity of the critical Reynolds number the required number of time iterations to achieve an asymmetric solution is very high. The explicit discretization yielded a much more rapid (in time) occurrence of bifurcation than the implicit ones. Many other ways to perturb numerically the flow have been attempted in the past but it is not likely that the characteristics of real flow perturbations can be known in detail. Regardless of this, different physical perturbations introduced numerically should all lead to the same final flow pattern and the one that results in the minimum computational time should be chosen, see Braza, Chassaing & Ha Minh (1986). Therefore, to reduce computational time, inlet perturbations were prescribed during a short time period and then removed. The numerical perturbations are not a sustained source of energy to the flow but rather a trigger mechanism to amplify the instability that bifurcates the solution to the Navier–Stokes equations. The method used to generate the perturbation was as follows:

(i) Solving the initial-value problem, the flow is accelerated from rest. The inlet conditions are therefore zero velocity and a parabolic profile for the V- and U-velocity components respectively:

(ii) After n time iterations and during m time iterations the inlet velocity profiles are changed as a function of time only for the U-velocity component, and as a function of time and space for the normal velocity component according to

$$U(u,t) = U(y)_{\text{fully developed}} + U(t), \tag{2}$$

where

$$U(t) = C_1\, U_{\max} \sin\left[2\pi\omega(t-t_0)\right]. \tag{3}$$

ω was equal to 1 to 10 Hz and the amplitude was chosen as high as $C_1 = 0.2$. The time at iteration m is denoted by t_0. The normal velocity component was prescribed as

$$V(y,t) = C_2\, U_{\max} \sin\left[2\pi\omega(t-t_0)\right] \sin\left[\pi(y-C_3-y_0)/C_3\right], \tag{4}$$

where

$$y_0 = C_4 \sin\left[2\pi(t-t_0)\right], \quad C_2 = 0 \rightarrow 0.05, \quad C_3 = 0.01, \quad C_4 = 0.001.$$

The above perturbation scheme was one of many different perturbations attempted. The steady-state solution however, was in no way influenced by the perturbation function and in this sense the perturbation was truly arbitrary.

The effect of the perturbations is illustrated in figure 3. In this figure the points of detachment or reattachment ($x_1, x_2, \ldots$) are shown as a function of time. Figure 3 (a) is computed for a Reynolds number of 70 and illustrates that the flow is stable in its symmetry and no bifurcation occurs during or after the period of perturbation.

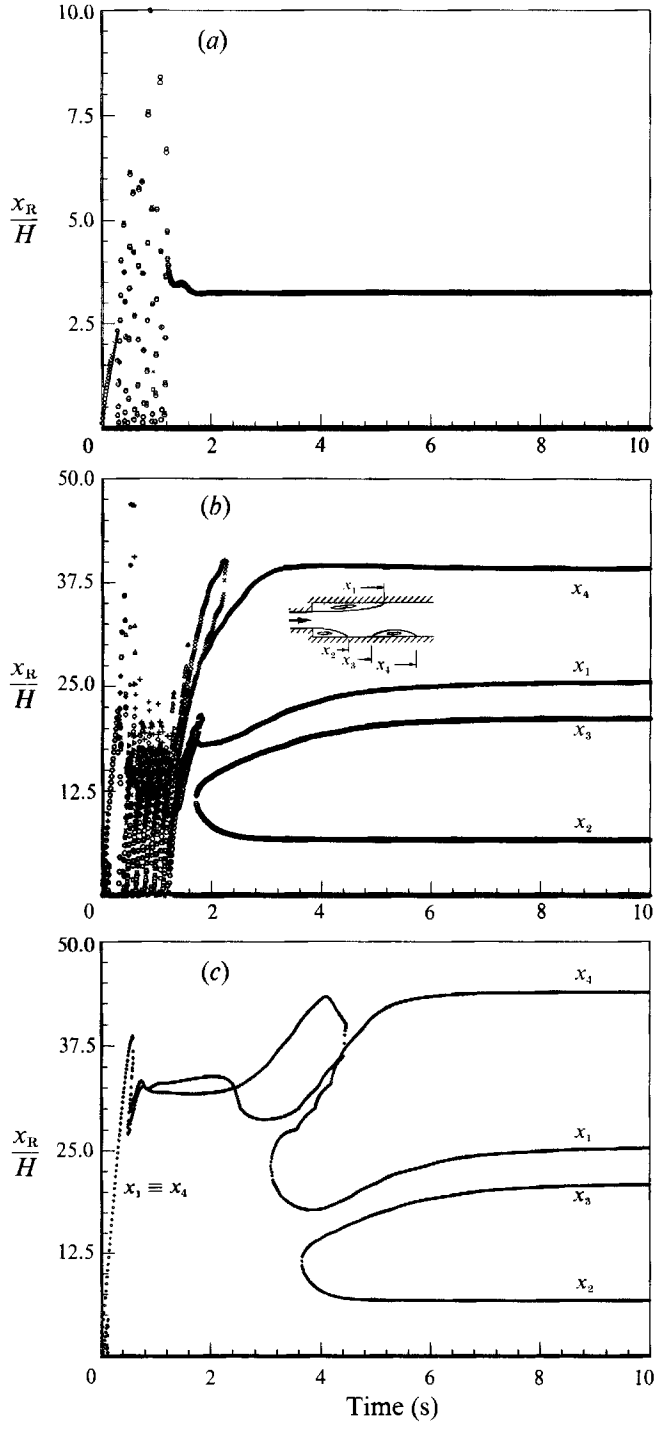

FIGURE 3. Calculated temporal evaluation of detachment and reattachment points: (*a*) $Re = 70$ without perturbation; (*b*) $Re = 610$ with perturbation; (*c*) $Re = 610$ without perturbation.

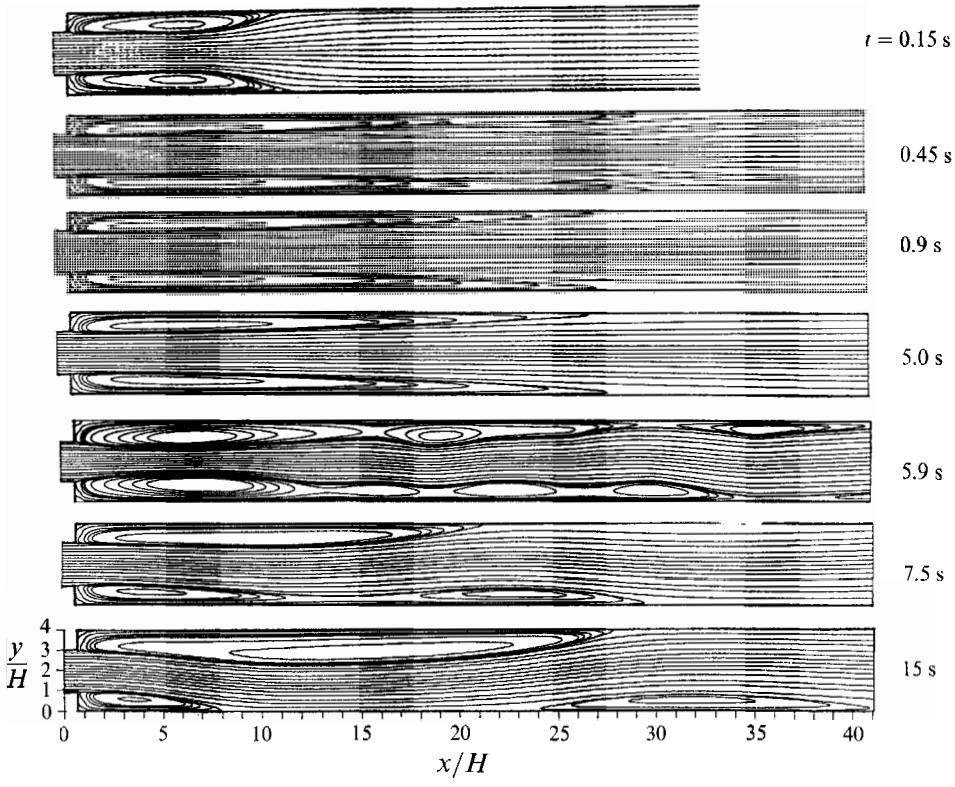

FIGURE 4. Calculated instantaneous streamlines for $Re = 610$.

Results for $Re = 610$ are shown in figure 3(*b*) and are representative also for those computed at $Re = 300$. Here the asymmetry is readily apparent as is the relative fast convergence to stationary lengths of the separation zones. This is apparent by comparing these results to those in figure 3(*c*), obtained without any prescribed perturbations in the computations. Not only does the asymmetry of the flow arise much later but even afterwards; the final lengths of the separation regions are not reached for a very long time. In fact over the time period shown in figure 3(*c*) the x_i values are still converging on their final values.

The large fluctuations of x_i values observed during the perturbation period in figure 3 correspond to the initial development of the flow field after the impulsive start. This is more clearly seen in the time series of streamline patterns shown in figure 4 for $Re = 610$. During this period the separation zones vary dramatically in length and position before reaching their steady-state condition.

4. Results and discussion

The global development of the steady flow obtained with increasing Reynolds numbers is summarized in the series of streamline patterns shown in figure 5. These results, obtained with the explicit Leith-type temporal discretization, shows the asymmetry of the flow starting at Reynolds numbers between 100 and 175. Above this Reynolds numbers the shorter separation region does not change significantly in length whereas the longer region grows almost linearly with Reynolds number. At Reynolds numbers above about 400 a third separation region appears on the short

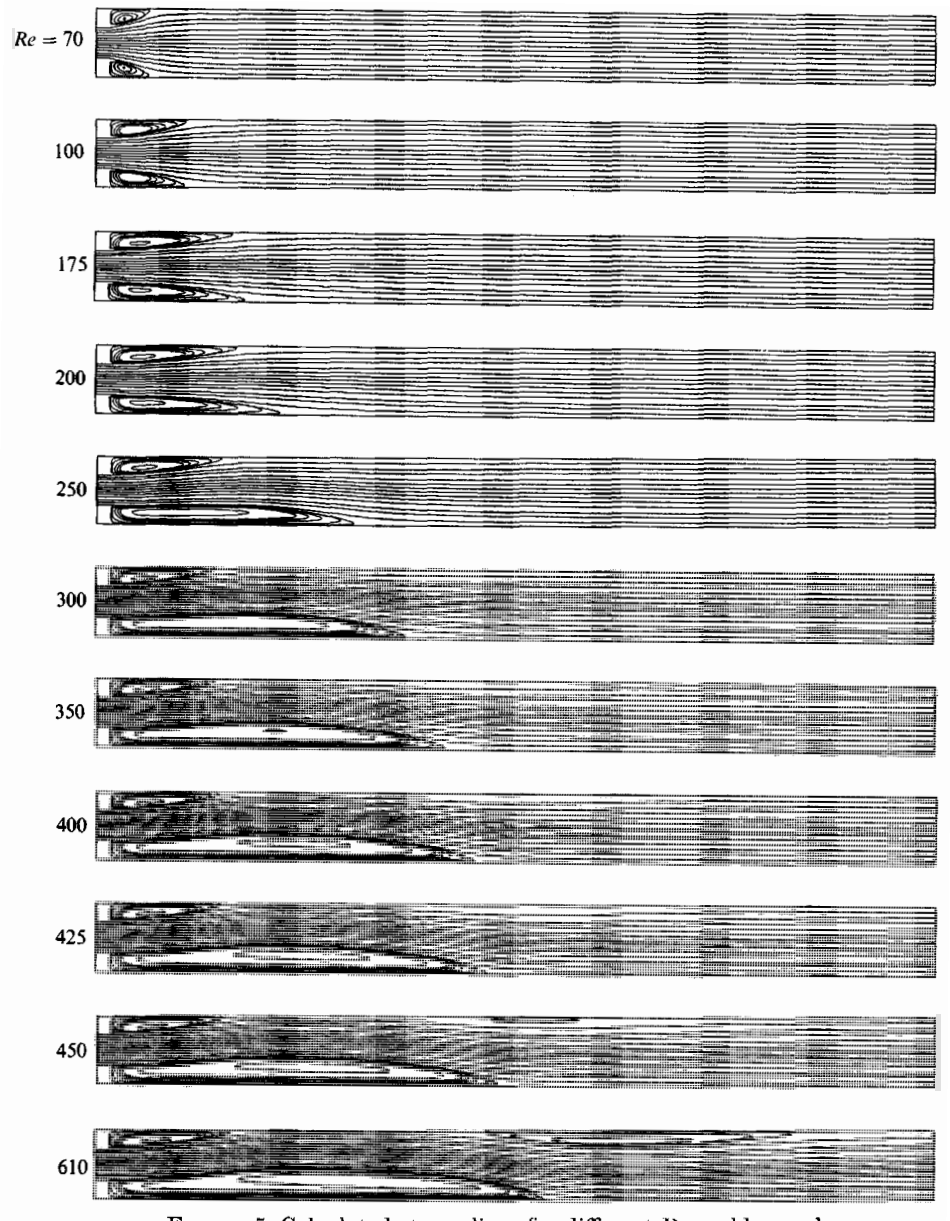

FIGURE 5. Calculated streamlines for different Reynolds numbers.

sidewall, growing in length with increasing Reynolds number, similar to the backward-facing step flow (see Armaly *et al.* 1983).

This flow development is shown in more condensed form in figure 6, in which the detachment and reattachment points are shown as a function of Reynolds number. Experimental results are also shown in this figure, indicating the good agreement between experiment and numerical predictions. One exception is the length x_1 at higher Reynolds numbers ($Re = 610$), which is predicted to be about 18% shorter than was observed in the measurements. No attempt was made experimentally to determine the lengths x_3 and x_4, although the onset of this separation region is seen in one of the measured velocity profiles (see figure 6). Finally a result labelled

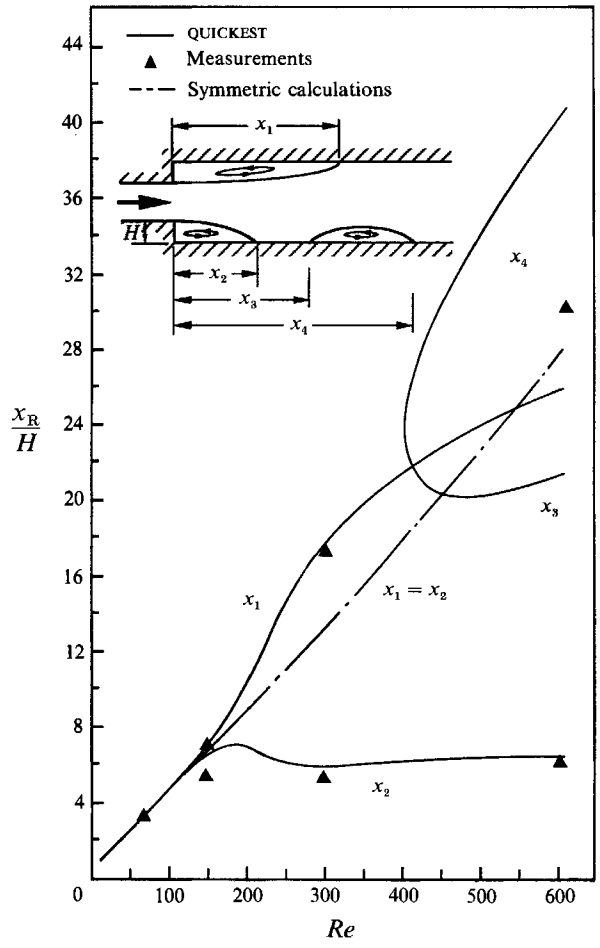

FIGURE 6. Summary of detachment and reattachment points as a function of Reynolds number.

symmetric calculations is shown in figure 6 for reference. These calculations were performed by using only half of the computational domain and treating the channel centreplane as a plane of symmetry, while still using 13-point quadratic upstream convection discretization scheme. As expected, the separation zone grows linearly with increasing Reynolds number.

The symmetry-breaking bifurcation seen in figure 5 is not a sudden transition which occurs over a small variation of Reynolds number but rather an asymptotic transition. This is illustrated more clearly in the bifurcation diagram shown in figure 7, in which the mean V-velocity component on the channel centreline is shown as a function of Reynolds number. For low Reynolds numbers, when the flow is symmetric, this velocity is zero. Deviations from zero occur as the flow becomes asymmetric, either positive or negative depending on the sense of the asymmetry. The transition from a value of zero to a non-zero value is, however, smooth and not abrupt as observed by Fearn *et al.* (1990). The actual point of bifurcation is therefore difficult to fix, but lies near a Reynolds number of 125.

Fearn *et al.* (1990) have shown similar results for a sudden expansion of ratio 1:3. Whereas they predict a sudden change to asymmetry, their experimental results

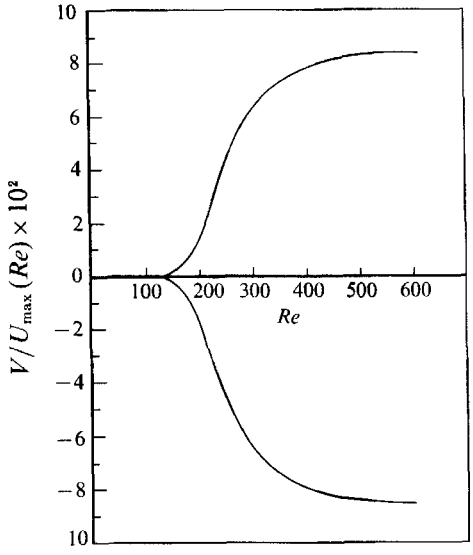

FIGURE 7. Calculated V-velocity on channel centreline.

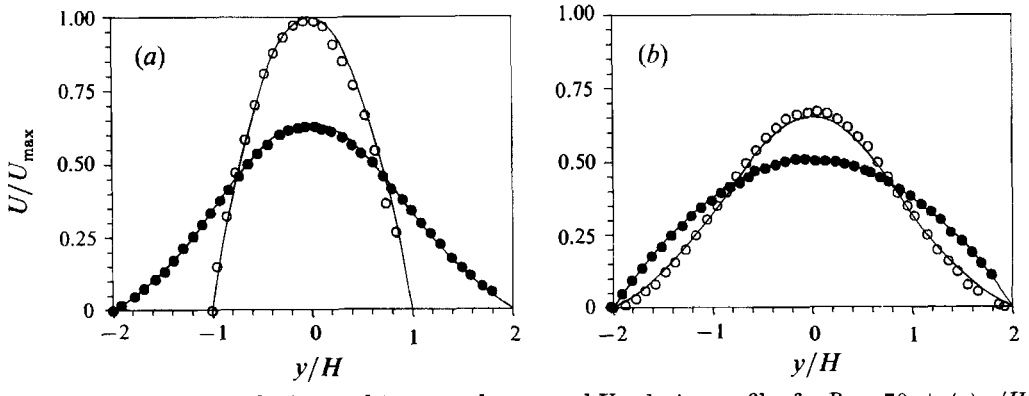

FIGURE 8. Comparison of calculated (——) and measured U-velocity profiles for $Re = 70$ at: (*a*) $x/H = -1.0$ (○), $x/H = 3.6$ (●); (*b*) $x/H = 5$ (○), $x/H = 14$ (●).

confirm the behaviour shown in figure 7. Fearn *et al.* were able to predict this behaviour by introducing a constant asymmetry of 1% into the sudden expansion geometry. Using the Reynolds number based on the upstream channel height, they observed flow asymmetry for Reynolds numbers exceeding about 64. The difference to the present value of 125 lies in the different expansion and aspect ratios used (see Chedron *et al.* 1978).

Finally some direct velocity comparisons between experimental data and numerical predictions are presented to illustrate the range and degree of accuracy. In figure 8, two selected downstream profiles for $Re = 70$ are shown. It is clear from these comparisons in the separation region and in the recovery region that the agreement between experiment and predictions is excellent throughout the entire flow region. Detailed comparisons for $Re = 300$ also show excellent agreement at all measurement planes. Therefore, the final set of results will only be shown for the case $Re = 610$.

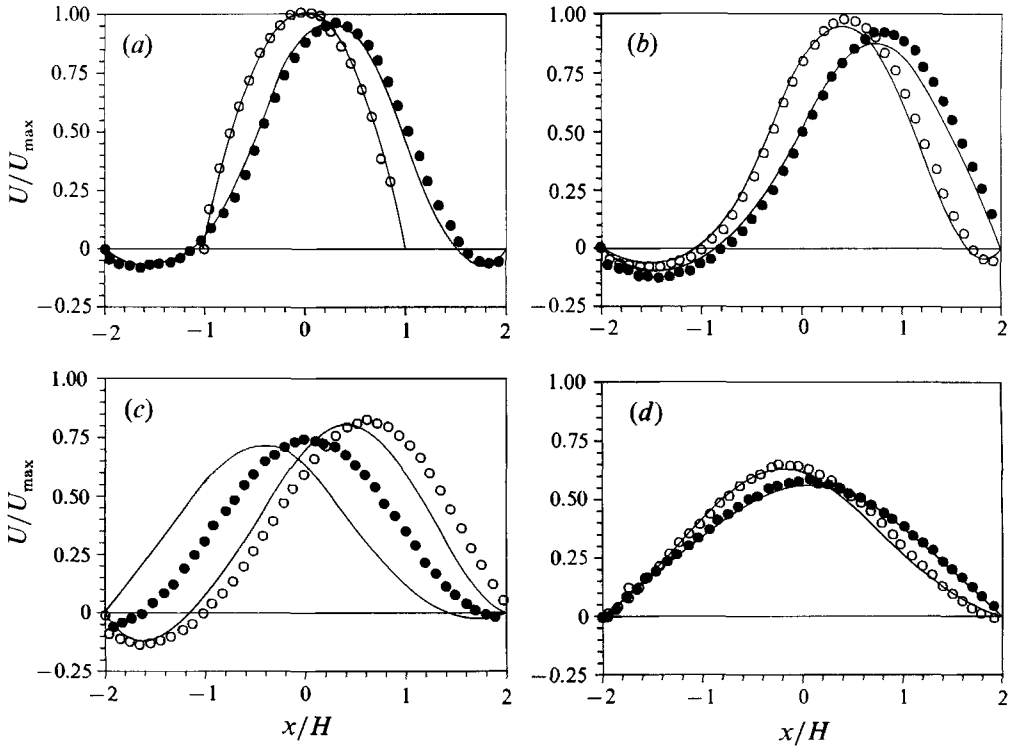

FIGURE 9. Comparison of calculated (——) and measured U-velocity profiles for $Re = 610$ at: (*a*) $x/H = -1$ (○), $x/H = 3.5$ (●); (*b*) $x/H = 5$ (○), $x/H = 14$ (●); (*c*) $x/H = 20$ (○), $x/H = 29$ (●); (*d*) $x/H = 44$ (○), $x/H = 60$ (●).

Figure 9 shows velocity profile comparisons at eight positions downstream of the expansion for $Re = 610$ and good agreement was obtained up to the third separated flow region. The largest deviations occur at $x/H = 29$ (figure 9*c*), the position where the third separation region is just starting. Up to $Re = 610$ a Hopf bifurcation was found neither in the predictions nor in the experiments. Since there is no fixed point of detachment for this separation zone, the assumption of flow two-dimensionality requires further study. As suggested by other authors, in non-periodic channels an unsteady period flow could be triggered after the appearance and development of flow three-dimensionality.

The present work was supported by the Deutsche Forschungsgemeinschaft within the Schwerpunktprogramm 'Finite Approximationen in der Strömungsmechanik'. The assistance of Mr K. Eichelberger in performing the experimental measurements is gratefully acknowledged.

Appendix. Numerical model

The Navier–Stokes equations are integrated over a time increment Δt and over the control volume v surrounding a grid node (see figure 10). The first term of the Navier–Stokes equations for $\phi = U_1, U_2$ yields

$$\int_t^{t+\Delta t} \int_v \phi_t \, \mathrm{d}v \, \mathrm{d}t = \int_{-\Delta y/2}^{\Delta y/2} \int_{-\Delta x/2}^{\Delta x/2} (\phi^{n+1} - \phi^n) \, \mathrm{d}\xi \, \mathrm{d}\eta = v(\tilde{\phi}^{n+1} - \tilde{\phi}^n), \qquad \text{(A 1)}$$

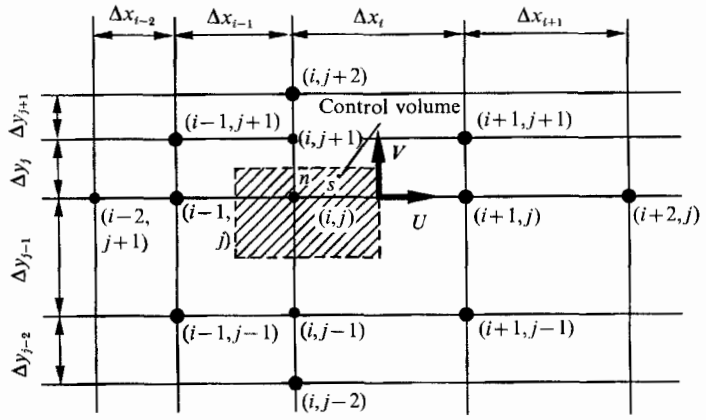

FIGURE 10. Control volume and notation used in the quadratic Leith type of temporal discretization together with the 13-point scheme.

where $\tilde{\phi}$ stands for the mean values in the control volume. Considering, for simplicity, a uniformly spaced mesh in both coordinate directions and further assuming that the dependent variable is defined in a local reference frame (ξ, η) by a quadratic function:

$$\phi = c_1 + c_2\xi + c_3\xi^2 + c_4\eta + c_5\eta^2 + c_6\xi\eta, \tag{A 2}$$

the mean values $\tilde{\phi}$ may be obtained as

$$\tilde{\phi} = \frac{1}{\Delta x\,\Delta y}\iint \phi\,\mathrm{d}\xi\,\mathrm{d}\eta = c_1 + \frac{c_3}{12}\Delta x^2 + \frac{c_5}{12}\Delta y^2 \tag{A 3}$$

and (A 1) appears as

$$\int_t^{t+\Delta t}\int_v \phi_t\,\mathrm{d}v\,\mathrm{d}t = v\left[(c_1^{n+1}-c_1^n) + \frac{\Delta x^2}{12}(c_3^{n+1}-c_3^n) + \frac{\Delta y^2}{12}(c_5^{n+1}-c_5^n)\right]. \tag{A 4}$$

However, $c_3 = \frac{1}{2}\partial^2\phi/\partial\xi^2$ and $c_5 = \frac{1}{2}\partial^2\phi/\partial\eta^2$, yielding

$$\frac{\Delta x^2}{12}(c_3^{n+1}-c_3^n) = \frac{\partial x^2}{24}\Delta t\left[\frac{\partial}{\partial t}\left(\frac{\partial^2\phi}{\partial\xi^2}\right)\right]. \tag{A 5}$$

Taking the second derivation of the Navier–Stokes equations and neglecting fourth-order derivatives, (A 4) becomes

$$\frac{\Delta x^2}{12}(c_3^{n+1}-c_3^n) = -\frac{\Delta x}{24}\Delta t\left[\frac{\partial^2(u\phi)}{\partial\xi^2}\right]_{i-\frac{1}{2},j}^{i+\frac{1}{2},j} = -\frac{\partial x}{24}\Delta t\,[2(c_3u)_{i+\frac{1}{2},j} - 2(c_3u)_{i-\frac{1}{2},j}]. \tag{A 6}$$

Replacing c_1, c_3 and c_5 by their values, referenced to the dependent variables in (ξ, η) yields

$$\int_t^{t+\Delta t}\int_v \phi_t\,\mathrm{d}v\,\mathrm{d}t = v\left\{(\phi_{i,j}^{n+1}-\phi_{i,j}^n) - \left[\frac{\Delta x^2}{24}(C_{i+\frac{1}{2},j}\,\mathrm{CURV}_{i+\frac{1}{2},j}^+ - C_{i-\frac{1}{2},j}\,\mathrm{CURV}_{i-\frac{1}{2},j}^+) + \frac{\Delta y^2}{24}(C_{i,j+\frac{1}{2}}\,\mathrm{CURV}_{i,j+\frac{1}{2}}^+ - C_{i,j-\frac{1}{2}}\,\mathrm{CURV}_{i,j-\frac{1}{2}}^+)\right]^n\right\}, \tag{A 7}$$

where $C_{i\pm\frac{1}{2},j\pm\frac{1}{2}}$ stand for the Courant numbers, e.g. $C_{i+\frac{1}{2},j} = u_{i+\frac{1}{2},j}\Delta t/\Delta x$, and $\mathrm{CURV}^{+}_{i\pm\frac{1}{2},j\pm\frac{1}{2}}$ denote finite difference approximations to a second derivative, e.g.

$$\mathrm{CURV}^{+}_{i+\frac{1}{2},j} = (\phi_{i-1,j}+\phi_{i+1,j}-2\phi_{i,j})/\Delta x^2. \tag{A 8}$$

The finite-difference counterpart of the convection and diffusion terms is evaluated as follows:

$$\int_t^{t+\Delta t}\int_\nu \left(\frac{\partial(u\phi)}{\partial\xi}-\nu\frac{\partial^2\phi}{\partial\xi^2}\right)\mathrm{d}\nu\,\mathrm{d}t = \int_t^{t+\Delta t}\left[u\phi-\nu\frac{\partial\phi}{\partial\xi}\right]_{i-\frac{1}{2},j}^{i+\frac{1}{2},j}\mathscr{A}\,\mathrm{d}t \tag{A 9}$$

and the first term may be written as

$$\int_t^{t+\Delta t}[u\phi]_{i-\frac{1}{2},j}^{i+\frac{1}{2},j}\mathscr{A}\,\mathrm{d}t = \int_t^{t+Dt}[u\phi]_{i+\frac{1}{2},j}\mathscr{A}\,\mathrm{d}t-\int_t^{t+\Delta t}[u\phi]_{i-\frac{1}{2},j}\mathscr{A}\,\mathrm{d}t. \tag{A 10}$$

For conciseness, only the convective flux at the $(i+\frac{1}{2},j)$ control volume face is discretized, considering $u_{i+\frac{1}{2},j} > 0$. Thus, replacing the temporal integration by Lagrangian integrals:

$$\int_t^{t+\Delta t}[u\phi]_{i+\frac{1}{2},j}\mathscr{A}\,\mathrm{d}t = \int_0^{\Delta\xi'}[\tilde{\phi}(\xi')]\mathscr{A}\,\mathrm{d}\xi', \tag{A 11}$$

where

$$\Delta\xi' = \int_{t+\Delta t}^{t} u_{i+\frac{1}{2},j}\,\mathrm{d}t = C_{i+\frac{1}{2},j}\Delta x,$$

and evaluating the mean value $\tilde{\phi}$ at the $(i+\frac{1}{2},j)$ control volume face, $\tilde{\phi} = c_1+c_2\xi'+c_3\xi'^2+\frac{1}{12}c_5\Delta y^2$, yields

$$\int_0^{\Delta\xi'}[\tilde{\phi}(\xi')]\mathscr{A}\,\mathrm{d}\xi' = \mathscr{A}\left[c_1\xi'+\frac{c_2}{2}\xi'^2+\frac{c_3}{3}\xi'^3+\frac{c_5}{12}\Delta y^2\xi'\right]_{\frac{1}{2}\Delta x-C_{i+\frac{1}{2},j}\Delta x}^{\frac{1}{2}\Delta x}. \tag{A 12}$$

The coefficients c_1, c_2, c_3 and c_5 are obtained from the quadratic function (A 2) at time t, oriented in an upwind like manner.

A similar procedure is followed for the diffusion fluxes. The mean value of the diffusive unit flux at the control volume face $(i+\frac{1}{2},j)$ is given in the Lagrangian space by $\partial\tilde{\phi}/\partial\xi' = c_2+2c_3\xi'$, leading to

$$\int_t^{t+\Delta t}\left[\nu\frac{\partial\tilde{\phi}}{\partial\xi}\right]_{i+\frac{1}{2},j}\mathscr{A}\,\mathrm{d}t = \int_0^{\Delta\xi'}\frac{\nu}{u_{i+\frac{1}{2},j}}\frac{\partial\tilde{\phi}}{\partial\xi'}\mathscr{A}\,\mathrm{d}\xi' = \left[\frac{\nu}{u_{i+\frac{1}{2},j}}(c_2\xi'+c_3\xi'^2)\right]_{\frac{1}{2}\Delta x-C_{i+\frac{1}{2},j}}^{\frac{1}{2}\Delta x}\Delta x. \tag{A 13}$$

The explicit finite differences are obtained by rearranging the resulting finite difference expressions and the explicit counterpart of source terms. Thus, the dependent variable at the $(n+1)$ time step for each control volume, is obtained from

$$\phi_{i,j}^{n+1} = \phi_{i,j}^{n}+(F_{i-\frac{1}{2},j}-F_{i+\frac{1}{2},j}+F_{i,j-\frac{1}{2}}-F_{i,j+\frac{1}{2}}+R_{i,j}+S_{i,j})^n, \tag{A 14}$$

where the fluxes, say e.g. $F_{i+\frac{1}{2},j}$, are given by $F_{i+\frac{1}{2},j} = \Psi_1+\Psi_2+\Psi_3$:

$$\Psi_1 = \mathscr{A}C_{i+\frac{1}{2},j}\Delta x\,[\tfrac{1}{2}(\phi_{i+1,j}+\phi_{i,j})-C_{i+\frac{1}{2},j}\tfrac{1}{2}(\phi_{i+1,j}-\phi_{i,j})], \tag{A 15}$$

$$\Psi_2 = \mathscr{A}\Delta x\,[-\tfrac{1}{6}\Delta x^2(1-C^2_{i+\frac{1}{2},j}-3\gamma)(\alpha\,\mathrm{CURV}^{+}_{i+\frac{1}{2},j}+\beta\,\mathrm{CURV}^{-}_{i+\frac{1}{2},j}) + \tfrac{1}{24}\Delta y^2(\alpha\,\mathrm{CURV}^{+}_{i,j+\frac{1}{2}}+\beta\,\mathrm{CURV}^{-}_{i,j+\frac{1}{2}})], \tag{A 16}$$

$$\Psi_3 = -\mathscr{A}\gamma\Delta x\,[(\phi_{i+1,j}-\phi_{i,j})-\tfrac{1}{2}\Delta x^2(\alpha\,\mathrm{CURV}^{+}_{i+\frac{1}{2},j}+\beta\,\mathrm{CURV}^{-}_{i+\frac{1}{2},j})], \tag{A 17}$$

where

$$\alpha = \tfrac{1}{2}(C_{i+\frac{1}{2},j} + |C_{i+\frac{1}{2},j}|) \quad \beta = \tfrac{1}{2}(C_{i+\frac{1}{2},j} - |C_{i+\frac{1}{2},j}|) \text{ and } \quad \gamma = \nu \Delta t / \Delta x^2.$$

The control-volume face area is represented by $\mathscr{A}$ and

$$R_{ij} = \nu(\Delta t/\Delta x)\,(p_{i-1,j} - p_{i,j}). \tag{A 18}$$

$S_{i,j}$ denotes the additional source terms. The velocity divergence for a control volume is driven approximately to zero by adjusting the control-volume pressure. The pressure adjustment (u') produces a corresponding velocity adjustment, which for the u-velocity component is determined, e.g. for $u_{i+\frac{1}{2},j}$, by

$$u'_{i+\frac{1}{2},j} = \frac{\Delta t}{\rho} \frac{(p'_{i,j} - p'_{i+1,j})}{\Delta x}. \tag{A 19}$$

The integration of the continuity equation and its discretization using the corrected velocity field $v = v^* + v'$ yields the finite difference equation for the pressure correction, resulting in the system of algebraic equations solved by the Stone's strong implicit method, see e.g. Azevedo, Durst & Pereira (1988).

REFERENCES

Acrivos, A. & Schrader, M. 1982 Steady flow in a sudden expansion at high Reynolds numbers. *Phys. Fluids* **25**, 923.

Armaly, B. F., Durst, F., Pereira, J. C. F. & Schönung, B. 1983 Experimental and theoretical investigations of backward facing step flow. *J. Fluid Mech.* **127**, 473.

Azevedo, J. L. T., Durst, F. & Pereira, J. C. F. 1988 Comparison of strongly implicit procedures for the solution of the fluid flow equations in finite difference form. *Appl. Math. Modelling* **12**, 51.

Braza, M., Chassaing, P. & Ha Minh, H. 1986 Numerical study and physical analysis of pressure and velocity fields in the wake of a circular cylinder. *J. Fluid Mech.* **165**, 79.

Cherdron, W., Durst, F. & Whitelaw, J. H. 1978 Asymmetric flows and instabilities in symmetric ducts with sudden expansions. *J. Fluid Mech.* **84**, 13–31.

Davis, R. W. & Moore, E. F. 1982 A numerical study of vortex shedding from rectangles. *J. Fluid Mech.* **116**, 475–506.

Durst, F., Melling, A. & Whitelaw, J. H. 1974 Low Reynolds number flow over a plane symmetric sudden expansion. *J. Fluid Mech.* **64**, 111–128.

Fearn, R. M., Mullin, T. & Cliffe, K. A. 1990 Nonlinear flow phenomena in a symmetric sudden expansion. *J. Fluid Mech.* **211**, 595–608.

Leonard, B. P. 1979 A stable and accurate convective modelling procedure based on quadratic upstream interpolation. *Compl. Meths. Appl. Mech. Engng* **19**, 59.

Obi, S., Peric, M. & Scheuerer, G. 1989 A finite volume calculation procedure for turbulent flows with second-order closure and collocated variable arrangement. *Proc. 7th Symp. on Turbulent Shear Flows, Stanford*, pp. 17.4-1–17.4-6.

Patankar, S. V. 1980 *Numerical Heat Transfer and Fluid Flow.* Hemisphere.

Restivo, A. & Whitelaw, J. H. 1978 Turbulence characteristics of the flow downstream of a symmetric, plane sudden expansion. *Trans. ASME* I: *J. Fluids Engng* **100**, 308.

Shapira, M., Degani, D. & Weihs, D. 1990 Stability and existence of multiple solutions for viscous flow in suddenly enlarged channels. *Computers Fluids* **18**, 239–258.

Sobey, I. J. 1985 Observation of waves during oscillatory channel flow. *J. Fluid Mech.* **151**, 395–406.

Sobey, I. J. & Drazin, P. G. 1986 Bifurcations of two-dimensional channel flows. *J. Fluid Mech.* **171**, 263.

Wille, R. & Fernholz, H. 1965 Report on the first European Mechanics Colloquium on the Coanda effect. *J. Fluid Mech.* **23**, 801–819.